

Dear Author,

Here are the proofs of your article.

- You can submit your corrections **online**, via **e-mail** or by **fax**.
- For **online** submission please insert your corrections in the online correction form. Always indicate the line number to which the correction refers.
- You can also insert your corrections in the proof PDF and **email** the annotated PDF.
- For fax submission, please ensure that your corrections are clearly legible. Use a fine black pen and write the correction in the margin, not too close to the edge of the page.
- Remember to note the **journal title**, **article number**, and **your name** when sending your response via e-mail or fax.
- **Check** the metadata sheet to make sure that the header information, especially author names and the corresponding affiliations are correctly shown.
- **Check** the questions that may have arisen during copy editing and insert your answers/ corrections.
- **Check** that the text is complete and that all figures, tables and their legends are included. Also check the accuracy of special characters, equations, and electronic supplementary material if applicable. If necessary refer to the *Edited manuscript*.
- The publication of inaccurate data such as dosages and units can have serious consequences. Please take particular care that all such details are correct.
- Please **do not** make changes that involve only matters of style. We have generally introduced forms that follow the journal's style. Substantial changes in content, e.g., new results, corrected values, title and authorship are not allowed without the approval of the responsible editor. In such a case, please contact the Editorial Office and return his/her consent together with the proof.
- If we do not receive your corrections **within 48 hours**, we will send you a reminder.
- Your article will be published **Online First** approximately one week after receipt of your corrected proofs. This is the **official first publication** citable with the DOI. **Further changes are, therefore, not possible.**
- The **printed version** will follow in a forthcoming issue.

Please note

After online publication, subscribers (personal/institutional) to this journal will have access to the complete article via the DOI using the URL: [http://dx.doi.org/\[DOI\]](http://dx.doi.org/[DOI]).

If you would like to know when your article has been published online, take advantage of our free alert service. For registration and further information go to: <http://www.springerlink.com>.

Due to the electronic nature of the procedure, the manuscript and the original figures will only be returned to you on special request. When you return your corrections, please inform us if you would like to have these documents returned.

Metadata of the article that will be visualized in OnlineFirst

ArticleTitle	Comparative study between computational and experimental results for binary rarefied gas flows through long microchannels	
Article Sub-Title		
Article CopyRight	Springer-Verlag (This will be the copyright line in the final PDF)	
Journal Name	Microfluidics and Nanofluidics	
Corresponding Author	Family Name	Szalmas
	Particle	
	Given Name	Lajos
	Suffix	
	Division	Department of Mechanical Engineering
	Organization	University of Thessaly
	Address	Pedion Areos, Volos, 38334, Greece
	Email	lszalmas@gmail.com
Author	Family Name	Pitakarnnop
	Particle	
	Given Name	Jeerasak
	Suffix	
	Division	INSA, UPS, Mines Albi, ISAE, ICA (Institut Clément Ader)
	Organization	Université de Toulouse
	Address	135 avenue de Rangueil, Toulouse, 31077, France
	Email	jeerasak.pitakarnnop@insa-toulouse.fr
Author	Family Name	Geoffroy
	Particle	
	Given Name	Sandrine
	Suffix	
	Division	INSA, UPS, Mines Albi, ISAE, ICA (Institut Clément Ader)
	Organization	Université de Toulouse
	Address	135 avenue de Rangueil, Toulouse, 31077, France
	Email	sandrine.geoffroy@insa-toulouse.fr
Author	Family Name	Colin
	Particle	
	Given Name	Stephane
	Suffix	
	Division	INSA, UPS, Mines Albi, ISAE, ICA (Institut Clément Ader)
	Organization	Université de Toulouse
	Address	135 avenue de Rangueil, Toulouse, 31077, France
	Email	stephane.colin@insa-toulouse.fr
Author	Family Name	Valougeorgis
	Particle	
	Given Name	Dimitris
	Suffix	

Division	Department of Mechanical Engineering
Organization	University of Thessaly
Address	Pedion Areos, Volos, 38334, Greece
Email	diva@mie.uth.gr

Schedule	Received	18 February 2010
	Revised	
	Accepted	19 April 2010

Abstract A comparative study between computational and experimental results for pressure-driven binary gas flows through long microchannels is performed. The theoretical formulation is based on the McCormack kinetic model and the computational results are valid in the whole range of the Knudsen number. Diffusion effects are taken into consideration. The experimental work is based on the Constant Volume Method, and the results are in the slip and transition regime. Using both approaches, the molar flow rates of the He–Ar gas mixture flowing through a rectangular microchannel are estimated for a wide range of pressure drops between the upstream and downstream reservoirs and several mixture concentrations varying from pure He to pure Ar. In all cases, a very good agreement is found, within the margins of the introduced modeling and measurement uncertainties. In addition, computational results for the pressure and concentration distributions along the channel are provided. As far as the authors are aware of, this is the first detailed and complete comparative study between theory and experiment for gaseous flows through long microchannels in the case of binary mixtures.

Keywords (separated by '-') Binary rarefied gas flows - McCormack model - Discrete velocity method - Flow rate measurement

Footnote Information

Journal: 10404
Article: 627



Author Query Form

**Please ensure you fill out your response to the queries raised below
and return this form along with your corrections**

Dear Author

During the process of typesetting your article, the following queries have arisen. Please check your typeset proof carefully against the queries listed below and mark the necessary changes either directly on the proof/online grid or in the 'Author's response' area provided below

Query	Details required	Author's response
Front matter	Please check and confirm the affiliations.	
Reference	Please check and confirm the publication year of Szalmas and Valougeorgis (2010).	

2 **Comparative study between computational and experimental**
3 **results for binary rarefied gas flows through long microchannels**

4 **Lajos Szalmas · Jeerasak Pitakarnnop ·**
5 **Sandrine Geoffroy · Stephane Colin ·**
6 **Dimitris Valougeorgis**

7 Received: 18 February 2010 / Accepted: 19 April 2010
8 © Springer-Verlag 2010

9 **Abstract** A comparative study between computational
10 and experimental results for pressure-driven binary gas
11 flows through long microchannels is performed. The the-
12 oretical formulation is based on the McCormack kinetic
13 model and the computational results are valid in the whole
14 range of the Knudsen number. Diffusion effects are taken
15 into consideration. The experimental work is based on the
16 Constant Volume Method, and the results are in the slip
17 and transition regime. Using both approaches, the molar
18 flow rates of the He–Ar gas mixture flowing through a
19 rectangular microchannel are estimated for a wide range of
20 pressure drops between the upstream and downstream
21 reservoirs and several mixture concentrations varying from
22 pure He to pure Ar. In all cases, a very good agreement is
23 found, within the margins of the introduced modeling and
24 measurement uncertainties. In addition, computational
25 results for the pressure and concentration distributions
26 along the channel are provided. As far as the authors are
27 aware of, this is the first detailed and complete comparative

study between theory and experiment for gaseous flows 28
through long microchannels in the case of binary mixtures. 29

Keywords Binary rarefied gas flows · 31
McCormack model · Discrete velocity method · 32
Flow rate measurement 33

1 Introduction 34

During the last decade, rarefied gas flows through long 35
channels have attracted considerable attention. This 36
increasing interest has been mainly stimulated by their 37
wide applicability in various technological fields including 38
the emerging field of nano- and microfluidics (Ho and Tai 39
1998; Kandlikar et al. 2006). In order to understand such 40
flows, both theoretical and experimental studies have been 41
carried out. 42

From theoretical standpoint, the most commonly applied 43
approaches include extended hydrodynamics (Colin 2005; 44
Szalmas 2007; Morini et al. 2005; Pitakarnnop et al. 2008; 45
Lockerby and Reese 2008), the DSMC method (Bird 1994; 46
Pitakarnnop et al. 2008), and kinetic theory, as specified by 47
the Boltzmann equation or alternatively by reliable kinetic 48
model equations (Ferziger and Kaper 1972; Cercignani 49
1988; Sharipov and Seleznev 1998). It has been shown that 50
for flows with small Mach numbers (such as the ones 51
investigated here) and the Knudsen number varying from the 52
free molecular through the transition up to the hydrody- 53
namic regimes, linearized kinetic theory is the most efficient 54
approach providing reliable results with modest computa- 55
tional effort. The discrete velocity method has been suc- 56
cessfully developed for solving such kinetic equations, 57
simulating flows through long channels of various cross 58
sections for both single component gases (Sharipov 1999; 59

A1 L. Szalmas (✉) · D. Valougeorgis
A2 Department of Mechanical Engineering, University of Thessaly,
A3 38334 Pedion Areos, Volos, Greece
A4 e-mail: lszalmas@gmail.com

A5 D. Valougeorgis
A6 e-mail: diva@mie.uth.gr

A7 J. Pitakarnnop · S. Geoffroy · S. Colin
A8 INSA, UPS, Mines Albi, ISAE, ICA (Institut Clément Ader),
A9 Université de Toulouse, 135 avenue de Rangueil,
A10 31077 Toulouse, France
A11 e-mail: jeerasak.pitakarnnop@insa-toulouse.fr

A12 S. Geoffroy
A13 e-mail: sandrine.geoffroy@insa-toulouse.fr

A14 S. Colin
A15 e-mail: stephane.colin@insa-toulouse.fr

60 Aoki 2001; Valougeorgis and Naris 2003; Breyiannis et al.
61 2008) and gaseous mixtures (Sharipov and Kalempa 2002;
62 Takata et al. 2003; Naris et al. 2004, 2005; Kosuge and
63 Takata 2008). In addition, in the case of one-dimensional
64 flows the semi-analytical discrete ordinate method has been
65 developed to solve kinetic equations associated with gas-
66 eous mixtures in a very elegant and computationally effi-
67 cient manner (Siewert and Valougeorgis 2004).

68 The experimental work for flows through long channels
69 has been based mainly on the Constant Volume and the
70 Droplet Tracking methods. By implementing the corre-
71 sponding test rigs, flow rates through various channels have
72 been measured (Harley et al. 1995; Zohar et al. 2002;
73 Maurer et al. 2003; Colin et al. 2004; Ewart et al. 2006,
74 2007; Marino 2009; Pitakarnnop et al. 2010). All those
75 studies, which also include comparisons between theory
76 and experiments, as well as efforts for estimating the
77 accommodation coefficients characterizing the gas-surface
78 interaction, have been focused on single component gases.
79 Recently, some of this studies has been applied to binary
80 gaseous mixtures (Pitakarnnop et al. 2010), where an
81 introductory comparison between theory and experiment
82 has been performed. However, in this latter study, the
83 comparison has been limited to $Kn < 0.05$, and even more,
84 it has been based on the measured and computed mass flow
85 rates and not on the molar flow rates, which as described
86 later, in the case of binary mixture flows, remain the proper
87 quantity for comparisons between computational and
88 experimental results.

89 In that framework, in this study, a detailed and systematic
90 comparison between computational and experimental
91 results for binary gas flows through long microchannels is
92 performed in the slip and transition regimes. In particular,
93 the flow configuration under investigation includes the
94 gaseous mixture of He–Ar flowing through a rectangular
95 microchannel for a wide range of pressure drops between the
96 upstream and downstream reservoirs and several mixture
97 concentrations varying from pure He to pure Ar. The
98 comparative study is based on the computed and measured
99 molar flow rates. The diffusion effects including the con-
100 centration variation along the channel are also considered in
101 the computations, and for several indicative cases, pressure
102 and concentration distributions along the channel are
103 provided.

104 In Sect. 2, the definition of the problem under investi-
105 gation is given, followed by the description of the com-
106 putational formulation and the experimental set up as
107 detailed in Sects. 3 and 4, respectively. In Sect. 5, the
108 comparative study based on the computed and measured
109 flow rates is presented, supplemented by some comple-
110 mentary computational results. Finally, concluding remarks
111 are presented in Sect. 6.

2 Definition of the problem

113 The isothermal pressure-driven flow of a binary gas mix-
114 ture through a microchannel, connecting two reservoirs, is
115 considered. The channel has rectangular cross section with
116 height $H = 1.88 \mu\text{m}$, width $W = 21.2 \mu\text{m}$, and length
117 $L = 5000 \mu\text{m}$, with H being the characteristic length. Since
118 $H, W \ll L$, end effects at the inlet and outlet of the channel
119 may be neglected. The channel axis lies in the z' direction,
120 while the cross section is in the x', y' coordinate sheet.

121 The gas mixture is consisting of two species, namely He
122 and Ar, having molecular masses $m_1 = 0.004003 \text{ kg/mol}$
123 and $m_2 = 0.03995 \text{ kg/mol}$, respectively. The concentration
124 of the light species in the gas mixture is defined by

$$C(z') = \frac{n_1(z')}{n_1(z') + n_2(z')}, \quad (1)$$

126 where $n_a(z')$, with $a = 1, 2$, denotes the molar density of the
127 two species, while $n = n_1 + n_2$ is the molar density of the
128 mixture. Index 1 refers always to He, since it is the lighter
129 gas compared to Ar. Also, from now on, we will refer to C as
130 the concentration of the gas mixture. Even more, the
131 molecular mass of the mixture is defined by

$$m(C) = Cm_1 + (1 - C)m_2. \quad (2)$$

133 Other quantities of the mixture of some importance in this
134 study are its viscosity $\mu(C)$ and the characteristic molecular
135 speed of the mixture $v(C) = \sqrt{2kT/m(C)}$, where
136 $k = 1.3807 \times 10^{-23} \text{ J/K}$ is the Boltzmann constant and T
137 a constant temperature characterizing the isothermal flow.
138 Also, the pressure of the mixture along the channel is given
139 by the equation of state

$$P(z') = n(z')kT. \quad (3)$$

141 It is seen that all quantities specified in this paragraph
142 (except m_1, m_2 , and T) depend explicitly or implicitly on z'
143 and, therefore, vary in the flow direction.

144 The pressure and concentration of the gas mixture in the
145 reservoirs are defined as (P_A, C_A) and (P_B, C_B) , with the
146 indexes A and B denoting the upstream and downstream
147 reservoirs, respectively. In this study, the flow is purely due
148 to an externally imposed pressure gradient and, therefore,
149 $P_A > P_B$, while $C_A = C_B$. The concentration C_A is taken as
150 the reference concentration of the gas mixture. It is
151 emphasized, that although the concentration of the mixture
152 at the two reservoirs is the same, a variation of the mixture
153 concentration along the channel may appear due to the fact
154 that the particles of the two species are traveling with
155 different molecular speeds. This phenomenon, known as
156 separation effect, has been discussed in the past by several
157 authors (Sharipov and Kalempa 2005; Takata et al. 2007;
158 Szalmas and Valougeorgis 2010). It is also noted that

160 during the flow process the concentration of the mixture in
 161 the reservoirs is considered as constant, since the number
 162 of gas molecules flowing through the channel is negligible
 163 compared to the gas molecules in the reservoirs.

164 Based on the above, the local dimensionless pressure
 165 and concentration gradients are defined as

$$X_P = \frac{H}{P} \frac{\partial P}{\partial z'} \quad \text{and} \quad X_C = \frac{H}{C} \frac{\partial C}{\partial z'}, \quad (4)$$

167 respectively.

168 A very important flow parameter is the local rarefaction
 169 parameter given by

$$\delta = \frac{P(z')H}{\mu(C)v(C)}, \quad (5)$$

171 with $P_A \leq P(z') \leq P_B$. The rarefaction parameter varies
 172 along the channel between the rarefaction parameters in the
 173 upstream and downstream reservoirs, denoted by δ_A and δ_B ,
 174 respectively. In general, the rarefaction parameter is pro-
 175 portional to the inverse Knudsen number. For the purposes
 176 of this study, the reference rarefaction parameter, $\delta_0 =$
 177 $(\delta_A + \delta_B)/2$ and the corresponding Knudsen number,
 178 $Kn_0 = 1/\delta_0$, are defined. As is seen from the definition of δ ,
 179 the Knudsen number is defined in terms of the channel height
 180 H , while the mean free path is defined via the mixture
 181 viscosity $\mu(C)$.

182 The quantity of major importance in this study, upon
 183 which the comparison study between theory and experi-
 184 ment is based, is the total molar flow rate defined as

$$J = J_1 + J_2, \quad (6)$$

186 which consists of the sum of the molar flow rates J_1 and J_2
 187 of He and Ar, respectively. The molar flow rates of each
 188 species are given by the integrals

$$J_\alpha = n_\alpha(z') \iint_{A'} u'_\alpha(x', y') dx' dy', \quad (7)$$

190 with $\alpha = 1, 2$, where $u'_\alpha(x', y')$ is the macroscopic velocity,
 191 and $A' = H \times W$ is the area of the cross section. It is seen,
 192 from Eq. 7, that the molar flow rates correspond to the
 193 amount of molecules in mol unit passing through a cross
 194 section of the channel per unit time. It is emphasized that
 195 although, at the right-hand side of Eq. 7, the molar density
 196 and the integral term vary along the flow, their product and,
 197 therefore, the molar flow rates J_1, J_2 , and J , due to particle
 198 conservation, remain invariant at each cross section. In the
 199 flow configuration presented here, this invariance of the
 200 molar flow rates at each cross section is always satisfied.

201 3 Computational approach

202 The solution of the flow of a binary gas mixture through a
 203 channel of rectangular cross section has been obtained in

Naris et al. (2005) in the whole range of the Knudsen 204
 number based on the McCormack kinetic model (McCormack 205
 1973). This model is considered as a reliable alterna- 206
 tive of the Boltzmann equation, since it satisfies all 207
 collision invariants, fulfills the H-theorem, and provides 208
 the correct expressions for all transport coefficients. It is 209
 also noted that while solving the viscous slip problem for 210
 binary gas mixtures, very good agreement has been found 211
 between the corresponding solutions of the linearized 212
 Boltzmann equation (Ivchenko et al. 1997) and of the 213
 McCormack model (Sharipov and Kalempa 2003) (see 214
 Table 2 in Sharipov and Kalempa (2003)). Of course, it is 215
 clarified that, strictly speaking, the present theoretical/ 216
 computational study is valid for monatomic dilute gas 217
 mixtures, which is also the case for the Boltzmann equa- 218
 tion. This description is well suited for rarefied gases. For 219
 the flow under consideration, i.e., binary gas flow through a 220
 rectangular channel an advanced discrete velocity algo- 221
 rithm (Naris et al. 2004a, b) has been applied in Naris et al. 222
 (2005) to solve the resulting system of linear integro-dif- 223
 ferential equations. The results are in dimensionless form 224
 and include the so-called kinetic coefficients. 225

In this study, the kinetic coefficients for the specific 226
 geometry, data and parameters imposed in the present flow 227
 configuration are computed. It is emphasized that the 228
 realistic potential (Kestin et al. 1984; Naris et al. 2004b, 229
 2005) is chosen for the computations. This model ensures 230
 the correct value of the binary gas mixture viscosity, which 231
 has been defined by applying the Chapman-Enskog theory 232
 to the McCormack model (Sharipov and Kalempa 2002). 233
 Even more, for the needs of this study, a methodology has 234
 been developed to convert the dimensionless results into 235
 dimensional molar flow rates, taking into account the 236
 variation of the flow quantities, including diffusion effects, 237
 along the channel. 238

To start with, the thermodynamic fluxes J_P and J_C 239
 conjugated to the thermodynamic forces X_P and X_C are 240
 introduced as (De Groot and Mazut 1984; Sharipov and 241
 Kalempa 2002) 242

$$J_P = -n \iint_{A'} w dx' dy', \quad (8)$$

$$J_C = -n_1 \iint_{A'} (u'_1 - u'_2) dx' dy', \quad (9) \quad 244$$

where 246

$$w(x', y') = \frac{n_1 u'_1 + n_2 u'_2}{n_1 + n_2} \quad (10)$$

is the averaged velocity. Also, it is noted that J_P and J_C are 248
 connected to the pressure and concentration gradients 249
 according to (Sharipov and Kalempa 2002; Naris et al. 250
 2005) 251

Author Proof

$$J_P = \frac{nA'v(C)}{2} [\Lambda_{PP}X_P + \Lambda_{PC}X_C], \quad (11)$$

$$J_C = \frac{nA'v(C)}{2} [\Lambda_{CP}X_P + \Lambda_{CC}X_C], \quad (12)$$

where Λ_{PP} , Λ_{CP} , Λ_{PC} , and Λ_{CC} , with $\Lambda_{CP} = \Lambda_{PC}$ due to the Onsager-Casimir relation, are the kinetic coefficients (Sharipov 1994). The kinetic formulation on the basis of J_P and J_C provides a theoretically well-established and convenient way of the problem definition.

It is useful to point that, in the formulation which follows, all four kinetic coefficients, which may contribute to the calculation of the molar flow rates J_1 and J_2 are considered. In particular, the coefficients Λ_{PP} and Λ_{CP} are due to the externally imposed pressure gradient, while the coefficients Λ_{PC} and Λ_{CC} are due to a concentration gradient along the channel, which is not externally imposed but is developed due to separation.

Using Eqs. 8–10 and the definition of the molar flow rates J_α , $\alpha = 1, 2$, given in Eq. 7, it is readily seen that

$$J_1 = -CJ_P - (1 - C)J_C, \quad (13)$$

$$J_2 = -(1 - C)(J_P - J_C). \quad (14)$$

Combining these expressions with Eqs. 11 and 12 and using the ideal gas law (see Eq. 3), the following system of equations is obtained (Szalmas and Valougeorgis 2010):

$$J_1 = -\frac{PA'H}{m(C)v(C)L} \left[(C\Lambda_{PP} + (1 - C)\Lambda_{CP}) \frac{\partial P}{\partial \hat{z}} \frac{1}{P} + (C\Lambda_{PC} + (1 - C)\Lambda_{CC}) \frac{\partial C}{\partial \hat{z}} \frac{1}{C} \right], \quad (15)$$

$$J_2 = -\frac{PA'H}{m(C)v(C)L} (1 - C) \left[(\Lambda_{PP} - \Lambda_{CP}) \frac{\partial P}{\partial \hat{z}} \frac{1}{P} + (\Lambda_{PC} - \Lambda_{CC}) \frac{\partial C}{\partial \hat{z}} \frac{1}{C} \right]. \quad (16)$$

where, $0 \leq \hat{z} \leq 1$, defined by $\hat{z} = z'/L$, is the non-dimensional coordinate along the axis of the channel. These equations are supplemented with the boundary conditions for the pressure and the concentration at the inlet and the outlet of the channel:

$$P(0) = P_A, \quad P(1) = P_B, \quad (17)$$

$$C(0) = C_A, \quad C(1) = C_B. \quad (18)$$

Equations 15 and 16 constitute a nonlinear system of two first-order ordinary differential equations, subject to (17) and (18). It can be solved to yield the unknown axial distributions $P = P(\hat{z})$ and $C = C(\hat{z})$, while the unknown flow rates J_α are defined by satisfying the conditions at $\hat{z} = 1$.

Finally, the solution of Eqs. 15 and 16 is carried out numerically. Initial estimates of J_1 and J_2 are provided

and then the system is solved by the Euler's method, starting from $\hat{z} = 0$ and with a discrete step $\Delta\hat{z}$ up to $\hat{z} = 1$. At each node along the channel, based on the values of the kinetic coefficients of the previous node, the values of P and C are estimated. Reaching the end of the channel at $\hat{z} = 1$, the computed values of the pressure and the concentration are compared to the corresponding boundary conditions. If the agreement is not satisfactory, then updated values of J_1 and J_2 based on the bisector method are provided, and the solution of the system is repeated. This iteration process terminates when some relative convergence criterion imposed on the outlet pressure and concentration is satisfied. Upon convergence, the distributions $P(\hat{z})$ and $C(\hat{z})$, as well as the quantities J_1 and J_2 are determined. Finally, the total flow rate J is calculated from J_α using Eq. 6.

As we conclude this section, the discretization parameters implemented in the computations are provided. The numerical algorithm used for the computation of the kinetic coefficients in Eqs. 15 and 16 is based on a computational grid consisting of 201×201 nodes for $Kn_0 \geq 1$, and 301×301 nodes for $Kn_0 < 1$ in the physical space, and of 64 magnitudes and 280 polar angles for all Knudsen numbers in the molecular velocity space. The iteration process for the estimation of the kinetic coefficients is terminated when the relative convergence error is less than 10^{-7} . Also, the Euler method involved in the solution of Eqs. 15 and 16 is based on a marching step of $\hat{z} = 1/500$, while the convergence criterion imposed on the outlet pressure and concentration is equal to 10^{-6} . Based on the above discretization, the results thus obtained are considered as accurate up to at least three significant figures.

4 Experimental approach

All the experimental data are obtained from an experimental setup described in Pitakarnnop et al. (2010), using the so-called Constant Volume Method. The microsystem is composed of a series of 45 identical microchannels etched by deep reactive ion etching (DRIE) in a silicon wafer, and closed by anodic bonding with a Pyrex plate. The height of the microchannels, $H = 1.88 \mu\text{m}$, has been measured by a TENCOR P1 profilometer, and the initial uncertainty of $\pm 0.1 \mu\text{m}$ was finally reduced to $\pm 0.01 \mu\text{m}$, after comparison between measured and simulated flow rates in the hydrodynamic regime, at low Knudsen numbers (Colin et al. 2004). The width of the microchannels is $W = 21.2 \pm 0.3 \mu\text{m}$, and their length is $L = 5000 \pm 10 \mu\text{m}$. The microchannels are connected to large upstream and downstream reservoirs, the constant volumes of which have been accurately measured using a specific setup, with an accuracy of $\pm 1.3\%$. During the flow of the gas through the

344 microsystem, the pressure inside each reservoir is measured
 345 by means of Inficon[®] capacitance diaphragm gauges, and the
 346 molar flow rates can be deduced from the ideal gas equation
 347 of state. The accuracy of the pressure measurements by the
 348 capacitance pressure gauges is 0.2% of reading. In order to
 349 maintain isothermal conditions, the setup is thermally reg-
 350 ulated by two Peltier modules, which allow maintaining a
 351 constant and uniform temperature inside the whole setup,
 352 i.e., inside the reservoirs as well as around the microsystem
 353 and all the connecting lines. Before each experiment, the
 354 whole circuit can be outgassed using a vacuum pump. Then,
 355 the upstream and downstream reservoirs are filled with the
 356 gas mixture from a high pressure tank. The pressure level is
 357 independently controlled in each reservoir with a pressure
 358 regulator. As soon as the waiting until thermal equilibrium is
 359 reached, valves are opened allowing the gas flow from the
 360 upstream to the downstream reservoir, through the micro-
 361 system. During the measure, upstream and downstream
 362 pressures are submitted to a small (typically 1–2%) decrease
 363 and increase, respectively. The temperature in the experi-
 364 ments is 298.5 K, and during operation, the temperature
 365 variation is measured with four PT100 temperature sensors
 366 (with a 0.15 K accuracy). Based on these measurements, the
 367 temperature standard deviation during each experiment is
 368 less than 0.1 K. Most of the setup is made of stainless steel,
 369 aluminum, or glass, and the connections are insured by ISO-
 370 KF and Swagelok Ultra-Torr[®] components to avoid any
 371 leakage during low pressure operation. Air tightness has
 372 been checked by means of helium detection, with a portable
 373 high precision leak detector.

374 From the measurement of the pressure variation in each
 375 reservoir, two experimental values of the molar flow rate
 376 can be deduced from

$$J_A^c = -\frac{dN_A}{dt} = -\frac{V_A}{R_g} \frac{d}{dt} \left(\frac{P_A}{T_A} \right), \quad J_B^c = \frac{dN_B}{dt} = \frac{V_B}{R_g} \frac{d}{dt} \left(\frac{P_B}{T_B} \right), \quad (19)$$

378 where t is the time, N_A and N_B are the amounts of gas
 379 molecules in mol units in the upstream and downstream
 380 reservoirs, respectively. P_A and T_A , P_B and T_B are the
 381 pressures and temperatures in these reservoirs of respective
 382 volumes V_A and V_B , and $R_g = k \times (6.022 \times 10^{23}/\text{mol})$ is
 383 the global gas constant. The experimental molar flow rate
 384 leaving the upstream reservoir is compared with the
 385 experimental molar flow rate entering the downstream
 386 reservoir. It is verified that deviation between the two
 387 values is well within the experimental uncertainty, and the
 388 average experimental molar flow rate can be defined as

$$J^c = \frac{J_A^c + J_B^c}{2}. \quad (20)$$

390 At this point, a discussion on the definition of the molar
 391 and mass flow rates is needed. In experiments with single

392 component gases, the mass flow rate dM/dt , instead of the
 393 molar flow rate dN/dt , is commonly introduced. Since, in
 394 general, $M = N \times m^*$, with m^* denoting the average
 395 molecular mass of the particles flowing through the
 396 channel during the experiment, the mass flow rate is
 397 obtained from Eq. 19 as

$$\frac{dM}{dt} = \pm \frac{V}{RT} \frac{dP}{dt}, \quad (21)$$

399 where, $R = k/m^*$ is the specific gas constant. For single
 400 component gases, the average mass m^* is equal to the
 401 molecular mass. However, for gaseous mixtures, m^* cannot
 402 be defined, since it refers to that gas portion which has
 403 flowed through the channel during the experiment. Because
 404 of the diffusion effects, that is the lighter particle has larger
 405 velocity than the heavier one, the concentration of this gas
 406 portion, denoted by C^* , is different from the concentrations
 407 in the two reservoirs (C_A and C_B), and it is not determined.
 408 In fact, this concentration can be expressed as $C^* = J_1 /$
 409 $(J_1 + J_2)$, and then the average mass is obtained by
 410 $m^* = C^*m_1 + (1 - C^*)m_2$. However, the component
 411 fluxes, J_1 and J_2 and consequently m^* , cannot be deter-
 412 mined from the present experimental approach. They are
 413 estimated only from the computational approach. There-
 414 fore, the experimental results and the comparative study
 415 are based on the molar and not on the mass flow rates.

416 Following from Eq. 19, the total molar flow rate through
 417 the channel is expressed by

$$J_A^c = -\frac{dN_A}{dt} = -\frac{V_A}{R_g T_A} \frac{dP_A}{dt} \left(1 - \frac{dT_A/T_A}{dP_A/P_A} \right), \quad (22)$$

$$J_B^c = \frac{dN_B}{dt} = \frac{V_B}{R_g T_B} \frac{dP_B}{dt} \left(1 - \frac{dT_B/T_B}{dP_B/P_B} \right).$$

419 As mentioned above, high-thermal stability is ensured by
 420 two temperature-regulation systems. The relative temperature
 421 variation dT/T is then, of the order of 4×10^{-4} , to be
 422 compared with the relative pressure variation $dP/$
 423 $P \approx 2 \times 10^{-2}$. As a consequence, Eq. 22 can be written as

$$J_A^c = -\frac{V_A}{R_g T_A} a_A c_A, \quad J_B^c = \frac{V_B}{R_g T_B} a_B c_B, \quad (23)$$

425 where $a = dP/dt$ is calculated from a least-square linear fit
 426 of the upstream or downstream measured pressure

$$P_A(t) = a_A t + b_A, \quad J_B^c = a_B t + b_B, \quad (24)$$

428 and $c = 1 - (dT/T)/(dP/P) = 1 \pm 2\%$. More than 1000
 429 pressure data are used for determining coefficients a and b .
 430 The standard deviation of coefficient a is calculated
 431 following the method proposed in Pitakarnnop et al.
 432 (2010) and is found to be less than 0.5%. Therefore, the
 433 overall uncertainty of the molar flow rate measurement is
 434 calculated from

$$\frac{\Delta J_A^c}{J_A^c} = \frac{\Delta J_B^c}{J_B^c} = \frac{\Delta V}{V} + \frac{\Delta T}{T} + \frac{\Delta a}{a} + \frac{\Delta c}{c}, \quad (25)$$

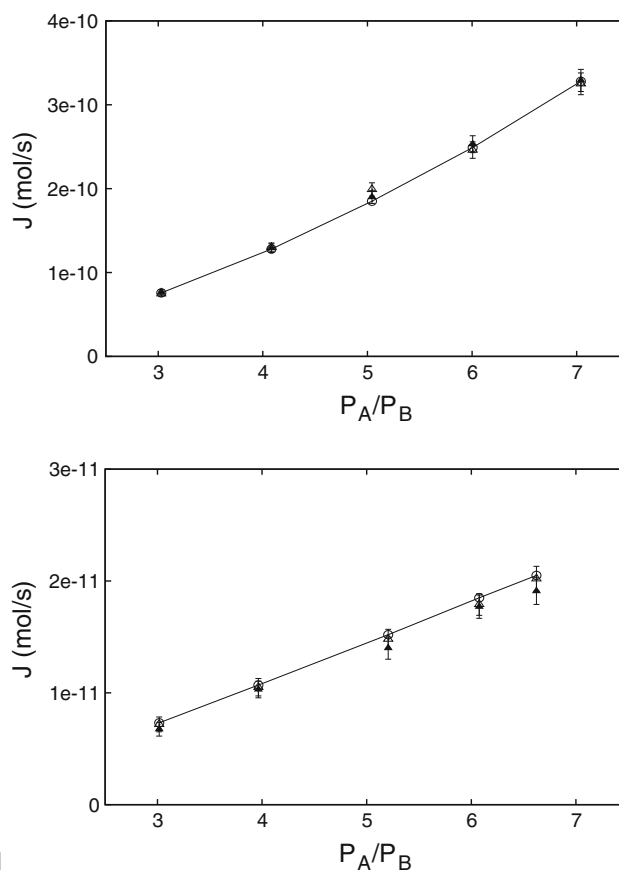
436 and is less than $\pm(1.3 + 0.2 + 0.5 + 2)\% = \pm 4\%$.
 437 Finally, it should be noted that outgassing from the setup
 438 when operating at low pressure could generally not be
 439 neglected, and, consequently, must be measured. In that
 440 case, a three-step procedure is used:

- 441 1. Outgassing is first quantified in the downstream circuit
 442 B, including reservoir B and all connections up to the
 443 microsystem outlet. In order to avoid flow through the
 444 microsystem during this operation, both upstream and
 445 downstream circuits are pressurized to the downstream
 446 operating pressure, and the valve placed between
 447 circuit A and the microchannel is closed. As soon as
 448 thermal stability is reached, the pressure rise in circuit
 449 B, which now is only due to outgassing, is measured.
- 450 2. After this step, pressure in the upstream circuit A is
 451 increased up to the desired upstream value and once
 452 thermal stability is reached, the pressure variations in
 453 circuits A and B are measured during the flow of the
 454 gas mixture from circuit A to circuit B through the
 455 microsystem.
- 456 3. Finally, outgassing is quantified in circuit A, including
 457 all connections up to the microsystem inlet. For this
 458 purpose, pressure in circuit B is increased to the same
 459 level as in circuit A, to avoid flow through the
 460 microsystem due to a pressure gradient, and the valve
 461 between circuit B and the microsystem is closed; then,
 462 the pressure rise in circuit A is monitored.

463 Outgassing rates in each circuit are calculated using
 464 Eqs. 23 and 24 and used to correct the flow rate data. The
 465 uncertainties shown in Eq. 25 are also taken into account
 466 for the calculation of the outgassed flow rate, and the total
 467 uncertainty represented by vertical bars in Figs. 1, 2, and 3
 468 takes into account all uncertainties introduced in the three
 469 steps of the operating procedure. As a consequence, when
 470 outgassing is not negligible, the total uncertainty is given
 471 by

$$\frac{\Delta J_A^c}{J_A^c} = \pm 0.04 \left(1 + 2 \frac{J_{ogA}^c}{J_A^c} \right), \quad \frac{\Delta J_B^c}{J_B^c} = \pm 0.04 \left(1 + 2 \frac{J_{ogB}^c}{J_B^c} \right), \quad (26)$$

473 where J_{ogA}^c is the molar flow rate due to outgassing in
 474 circuit A calculated from the third step of the procedure,
 475 and J_{ogB}^c is the molar flow rate due to outgassing in circuit
 476 B calculated from the first step of the procedure. The
 477 coefficient 2 in the brackets of the right-hand side terms of
 478 Eq. 26 is due to the fact that outgassing occurs in steps 2
 479 and 3 (respectively 1 and 2) necessary for calculating J_A^c
 480 (respectively J_B^c). It should be outlined that outgassing is
 481 essentially due to the manufactured parts of circuits A and



482 **Fig. 1** Computational and experimental total molar flow rates of
 483 He–Ar ($C_A = 0.1017$), with (i) $P_B \approx 15$ kPa (up) and (ii)
 484 $P_B \approx 2$ kPa (down). The symbols circle, open triangle, and filled
 485 triangle represent J , J_A^c , and J_B^c , respectively. The solid line is plotted
 486 to guide the eyes for the computational results of J

487 B, although outgassing from the walls of the microchannels
 488 can be neglected, first because silicon and glass wafers
 489 have very clean surfaces and second because the surface
 490 area of the microchannels walls is typically ten orders
 491 of magnitude lower than the total surface area of circuits A or
 492 B.

483 Finally, the comparison of the upstream and downstream
 484 resulting flow rates J_A^c and J_B^c is an indirect mean for ver-
 485 ifying that the outgassing effects are well taken into
 486 account by the procedure described above, whatever the
 487 level of outgassing.

493 5 Results

494 Computational and experimental results in tabulated and
 495 graphical form are provided for the flow of the He–Ar gas-
 496 ous mixture through the microsystem consisting of a series
 497 of 45 identical rectangular microchannels. The reference
 498 concentration C_A of the gas mixture, which as defined

499 before, refers to the concentration of He in the mixture varies
 500 between zero and one, taking the following values:
 501 $C_A = [0.0, 0.1017, 0.3012, 0.5010, 0.7019, 0.9014, 1.0]$.
 502 These values cover the whole range of the concentration
 503 interval from pure Ar ($C_A = 0$) to pure He ($C_A = 1$). For
 504 these values of exact concentration, the corresponding
 505 uncertainties are $[0, \pm 0.002, \pm 0.006, \pm 0.010, \pm 0.006,$
 506 $\pm 0.002, 0]$, respectively. The effect of the concentration
 507 uncertainty on the numerical calculations has been verified,
 508 and it was found that the introduced uncertainty for the flow
 509 rates is less than $\pm 0.5\%$. Two values of downstream pres-
 510 sure P_B , namely, $P_B \approx 15$ kPa and $P_B \approx 2$ kPa, are con-
 511 sidered. In both cases, the upstream to downstream pressure

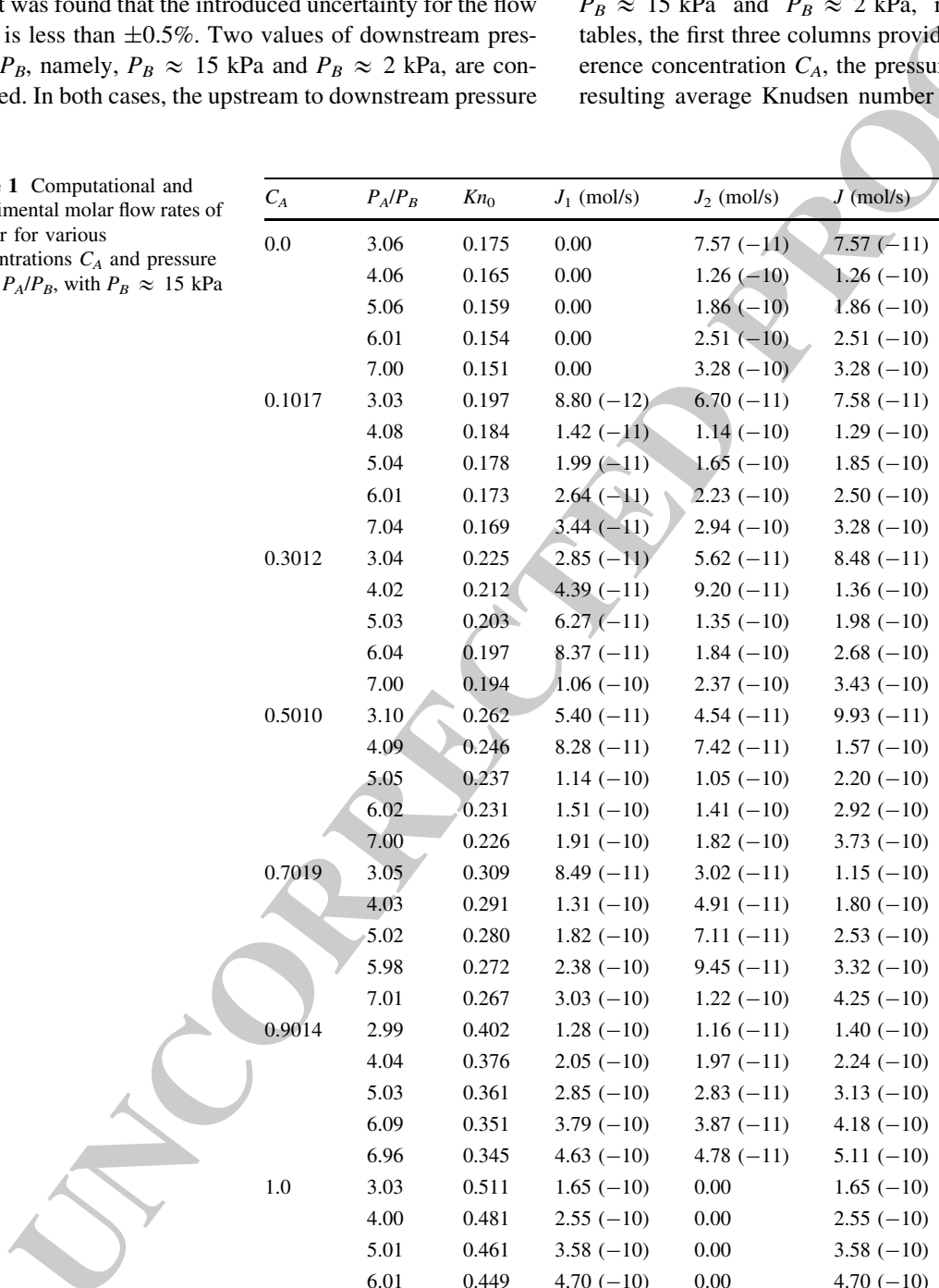
ratio varies approximately from three to seven. Therefore, 512
 the results are presented into two groups depending on P_B . 513
 The average Knudsen number varies in the first group with 514
 $P_B \approx 15$ kPa, as $0.1 < Kn_0 < 0.6$, and in the second group 515
 with $P_B \approx 2$ kPa, as $1.0 < Kn_0 < 4.0$. It is seen that the 516
 largest portion of the transition regime is covered. Results in 517
 the slip regime may be found in Pitakarnnop et al. (2010). 518

Based on the above flow parameters, Tables 1 and 2 519
 present computational and experimental flow rates for 520
 $P_B \approx 15$ kPa and $P_B \approx 2$ kPa, respectively. In these 521
 tables, the first three columns provide the values of the ref- 522
 erence concentration C_A , the pressure ratio P_A/P_B , and the 523
 resulting average Knudsen number Kn_0 , respectively. For 524

Table 1 Computational and experimental molar flow rates of He–Ar for various concentrations C_A and pressure ratios P_A/P_B , with $P_B \approx 15$ kPa

C_A	P_A/P_B	Kn_0	J_1 (mol/s)	J_2 (mol/s)	J (mol/s)	J^e (mol/s)	Δ
0.0	3.06	0.175	0.00	7.57 (–11)	7.57 (–11)	7.28 (–11)	3.97
	4.06	0.165	0.00	1.26 (–10)	1.26 (–10)	1.21 (–10)	3.62
	5.06	0.159	0.00	1.86 (–10)	1.86 (–10)	1.79 (–10)	3.40
	6.01	0.154	0.00	2.51 (–10)	2.51 (–10)	2.43 (–10)	3.45
	7.00	0.151	0.00	3.28 (–10)	3.28 (–10)	3.13 (–10)	4.90
0.1017	3.03	0.197	8.80 (–12)	6.70 (–11)	7.58 (–11)	7.56 (–11)	0.23
	4.08	0.184	1.42 (–11)	1.14 (–10)	1.29 (–10)	1.29 (–10)	–0.77
	5.04	0.178	1.99 (–11)	1.65 (–10)	1.85 (–10)	1.94 (–10)	–4.79
	6.01	0.173	2.64 (–11)	2.23 (–10)	2.50 (–10)	2.49 (–10)	0.15
	7.04	0.169	3.44 (–11)	2.94 (–10)	3.28 (–10)	3.26 (–10)	0.50
0.3012	3.04	0.225	2.85 (–11)	5.62 (–11)	8.48 (–11)	8.38 (–11)	1.16
	4.02	0.212	4.39 (–11)	9.20 (–11)	1.36 (–10)	1.36 (–10)	0.19
	5.03	0.203	6.27 (–11)	1.35 (–10)	1.98 (–10)	2.00 (–10)	–0.80
	6.04	0.197	8.37 (–11)	1.84 (–10)	2.68 (–10)	2.70 (–10)	–0.50
	7.00	0.194	1.06 (–10)	2.37 (–10)	3.43 (–10)	3.42 (–10)	0.24
0.5010	3.10	0.262	5.40 (–11)	4.54 (–11)	9.93 (–11)	9.80 (–11)	1.38
	4.09	0.246	8.28 (–11)	7.42 (–11)	1.57 (–10)	1.59 (–10)	–1.03
	5.05	0.237	1.14 (–10)	1.05 (–10)	2.20 (–10)	2.16 (–10)	1.41
	6.02	0.231	1.51 (–10)	1.41 (–10)	2.92 (–10)	2.90 (–10)	0.48
	7.00	0.226	1.91 (–10)	1.82 (–10)	3.73 (–10)	3.73 (–10)	–0.18
0.7019	3.05	0.309	8.49 (–11)	3.02 (–11)	1.15 (–10)	1.07 (–10)	7.24
	4.03	0.291	1.31 (–10)	4.91 (–11)	1.80 (–10)	1.73 (–10)	4.15
	5.02	0.280	1.82 (–10)	7.11 (–11)	2.53 (–10)	2.39 (–10)	5.69
	5.98	0.272	2.38 (–10)	9.45 (–11)	3.32 (–10)	3.15 (–10)	5.60
	7.01	0.267	3.03 (–10)	1.22 (–10)	4.25 (–10)	4.09 (–10)	3.96
0.9014	2.99	0.402	1.28 (–10)	1.16 (–11)	1.40 (–10)	1.38 (–10)	1.24
	4.04	0.376	2.05 (–10)	1.97 (–11)	2.24 (–10)	2.23 (–10)	0.80
	5.03	0.361	2.85 (–10)	2.83 (–11)	3.13 (–10)	3.11 (–10)	0.57
	6.09	0.351	3.79 (–10)	3.87 (–11)	4.18 (–10)	4.17 (–10)	0.04
	6.96	0.345	4.63 (–10)	4.78 (–11)	5.11 (–10)	5.09 (–10)	0.46
1.0	3.03	0.511	1.65 (–10)	0.00	1.65 (–10)	1.68 (–10)	–2.15
	4.00	0.481	2.55 (–10)	0.00	2.55 (–10)	2.57 (–10)	–0.94
	5.01	0.461	3.58 (–10)	0.00	3.58 (–10)	3.65 (–10)	–1.90
	6.01	0.449	4.70 (–10)	0.00	4.70 (–10)	4.77 (–10)	–1.42
	6.94	0.440	5.83 (–10)	0.00	5.83 (–10)	6.00 (–10)	–2.74

Author Proof



525 each concentration examined, five different pressure ratios
 526 are considered. The fourth and fifth columns provide the
 527 computational results of the molar flow rates of each species,
 528 J_1 and J_2 , followed in the sixth column with the total computa-
 529 tional flow rate $J = J_1 + J_2$. The flow rates are pre-
 530 sented in a normalized floating-point form. All values are
 531 given with an accuracy of three significant figures, and the
 532 exponents with base 10 are provided in brackets. This
 533 notation is common in rarefied gas calculations. The
 534 experimental total molar flow rates, denoted by J^c are given
 535 in the seventh column, while in the last column of both tables
 536 (column 8 in Table 1 and column 10 in Table 2), the relative

537 deviation between J and J^c , defined as $\Delta = 100(J/J^c - 1)$, is
 538 shown. Finally, the total experimental uncertainties are
 539 provided. The uncertainty for the experimental molar flow
 540 rates in Table 1 with $P_B \approx 15$ kPa, where outgassing is
 541 negligible, is in all cases $\pm 4\%$. However, the uncertainties
 542 for the results in Table 2 with $P_B \approx 2$ kPa, where outgas-
 543 sing is not negligible, is case dependent. In this latter situ-
 544 ation, the uncertainties for the inlet and outlet flow rates,
 545 denoted by ΔJ_A^c and ΔJ_B^c , are given in percentages in the
 546 eighth and ninth columns of Table 2.

547 Comparing the quantities in Table 1 with those in
 548 Table 2, it is seen that in Table 1, the average Knudsen

Table 2 Computational and experimental molar flow rates of He–Ar for various concentrations C_A and pressure ratios P_A/P_B , with $P_B \approx 2$ kPa

C_A	P_A/P_B	Kn_0	J_1 (mol/s)	J_2 (mol/s)	J (mol/s)	J^c (mol/s)	ΔJ_A^c	ΔJ_B^c	Δ
0.0	3.10	1.31	0.00	6.56 (–12)	6.56 (–12)	6.51 (–12)	9.67	9.58	0.82
	4.02	1.26	0.00	9.31 (–12)	9.31 (–12)	8.86 (–12)	8.59	8.56	5.02
	4.79	1.18	0.00	1.22 (–11)	1.22 (–11)	1.20 (–11)	7.30	7.76	1.93
	5.96	1.17	0.00	1.59 (–11)	1.59 (–11)	1.51 (–11)	6.84	7.50	4.97
	6.61	1.11	0.00	1.89 (–11)	1.89 (–11)	1.83 (–11)	6.03	6.55	3.08
0.1017	3.02	1.48	1.47 (–12)	5.85 (–12)	7.32 (–12)	6.96 (–12)	9.24	9.14	5.20
	3.96	1.39	2.05 (–12)	8.68 (–12)	1.07 (–11)	1.03 (–11)	7.42	7.22	3.65
	5.21	1.32	2.73 (–12)	1.25 (–11)	1.52 (–11)	1.44 (–11)	5.95	7.09	5.88
	6.08	1.29	3.18 (–12)	1.53 (–11)	1.85 (–11)	1.78 (–11)	5.40	5.88	3.93
	6.62	1.28	3.44 (–12)	1.71 (–11)	2.05 (–11)	1.97 (–11)	5.50	6.25	4.33
0.3012	3.07	1.68	4.76 (–12)	5.00 (–12)	9.76 (–12)	8.82 (–12)	7.90	8.33	10.6
	4.03	1.58	6.67 (–12)	7.44 (–12)	1.41 (–11)	1.27 (–11)	6.44	6.95	10.8
	5.00	1.52	8.43 (–12)	9.98 (–12)	1.84 (–11)	1.75 (–11)	5.75	5.60	5.34
	5.94	1.50	9.94 (–12)	1.24 (–11)	2.23 (–11)	2.12 (–11)	5.39	5.53	5.30
	6.67	1.45	1.13 (–11)	1.47 (–11)	2.60 (–11)	2.40 (–11)	5.19	5.83	8.17
0.5010	3.03	1.97	8.38 (–12)	3.78 (–12)	1.22 (–11)	1.13 (–11)	6.12	6.35	7.11
	4.06	1.85	1.21 (–11)	5.80 (–12)	1.79 (–11)	1.66 (–11)	5.20	5.66	7.45
	5.03	1.78	1.54 (–11)	7.81 (–12)	2.32 (–11)	2.11 (–11)	4.80	5.27	9.76
	5.91	1.73	1.82 (–11)	9.72 (–12)	2.79 (–11)	2.54 (–11)	4.67	5.11	10.06
	6.42	1.71	1.98 (–11)	1.09 (–11)	3.07 (–11)	2.83 (–11)	4.71	4.92	8.23
0.7019	3.06	2.32	1.29 (–11)	2.50 (–12)	1.54 (–11)	1.41 (–11)	5.63	5.78	9.22
	3.94	2.20	1.78 (–11)	3.67 (–12)	2.15 (–11)	2.00 (–11)	4.92	5.22	7.05
	5.42	2.07	2.58 (–11)	5.77 (–12)	3.16 (–11)	2.90 (–11)	4.59	4.95	8.92
	5.87	2.05	2.81 (–11)	6.43 (–12)	3.46 (–11)	3.13 (–11)	4.50	4.89	10.6
	6.33	2.03	3.05 (–11)	7.15 (–12)	3.77 (–11)	3.41 (–11)	4.46	4.83	10.4
0.9014	3.01	3.01	1.78 (–11)	8.97 (–13)	1.87 (–11)	1.80 (–11)	5.47	5.53	3.63
	3.95	2.83	2.56 (–11)	1.37 (–12)	2.70 (–11)	2.60 (–11)	4.86	5.05	3.79
	5.20	2.70	3.56 (–11)	2.06 (–12)	3.77 (–11)	3.56 (–11)	4.66	5.18	5.77
	5.88	2.64	4.11 (–11)	2.46 (–12)	4.35 (–11)	4.08 (–11)	4.43	4.74	6.67
	6.31	2.62	4.45 (–11)	2.71 (–12)	4.72 (–11)	4.53 (–11)	4.27	4.61	4.11
1.0	3.12	3.95	2.12 (–11)	0.00	2.12 (–11)	1.95 (–11)	6.63	6.44	9.04
	3.92	3.61	2.99 (–11)	0.00	2.99 (–11)	2.77 (–11)	5.58	5.96	7.81
	4.97	3.44	4.04 (–11)	0.00	4.04 (–11)	3.82 (–11)	5.05	5.34	5.69
	5.83	3.40	4.83 (–11)	0.00	4.83 (–11)	4.62 (–11)	4.83	5.02	4.41
	6.81	3.34	5.76 (–11)	0.00	5.76 (–11)	5.45 (–11)	4.52	4.92	5.74

549 numbers and flow rates are about one order of magnitude
 550 smaller than the ones in Table 2. The deviation Δ in Table 1
 551 varies between -4.79 and 7.24% with an average value of
 552 1.07% , while in Table 2 it is between 0.82 and 10.8% with
 553 the average value equal to 6.41% . It is seen that in the latter
 554 case the experimental results are always less than the cor-
 555 responding computational ones. Also, in general, the devi-
 556 ations Δ in Table 1 are much smaller than the corresponding
 557 ones in Table 2.

558 A complementary picture on the comparison between
 559 computational and experimental results, may be obtained
 560 by examining Figs. 1, 2, and 3, where results are provided
 561 for $C_A = 0.1017, 0.5010,$ and $0.9014,$ respectively. In these
 562 figures in addition to the computational total flow rates $J,$
 563 the corresponding experimental ones at the inlet and outlet
 564 reservoirs J_A^c and $J_B^c,$ respectively, with their associated bars
 565 of uncertainty are presented. It is clearly observed that in
 566 all cases the agreement between the results is much better
 567 for $P_B \approx 15$ kPa rather than for $P_B \approx 2$ kPa. In particular,
 568 for $P_B \approx 15$ kPa, the computational results are always
 569 well within the dispersion range of the experimental

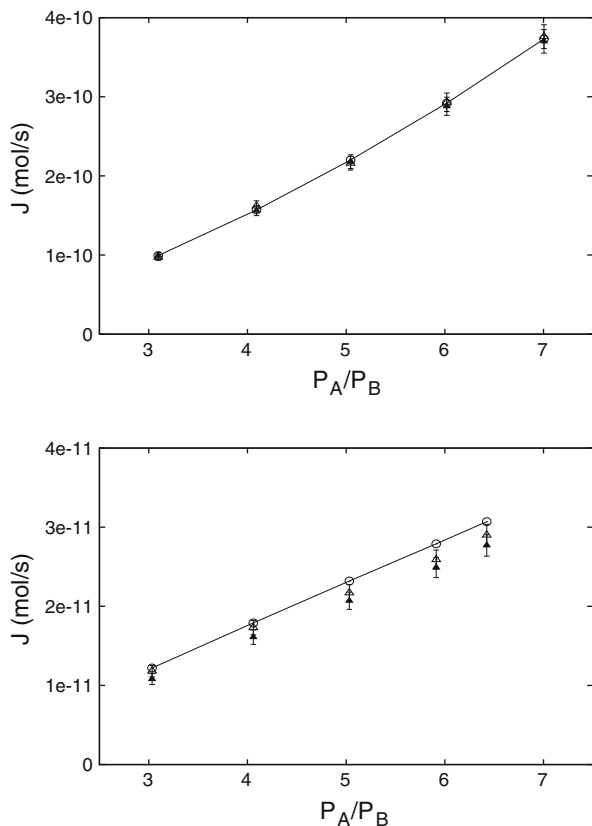


Fig. 2 Computational and experimental total molar flow rates of He-Ar ($C_A = 0.5010$), with (i) $P_B \approx 15$ kPa (up) and (ii) $P_B \approx 2$ kPa (down). The symbols open circle, open triangle, and filled triangle represent $J, J_A^c,$ and $J_B^c,$ respectively. The solid line is plotted to guide the eyes for the computational results of J

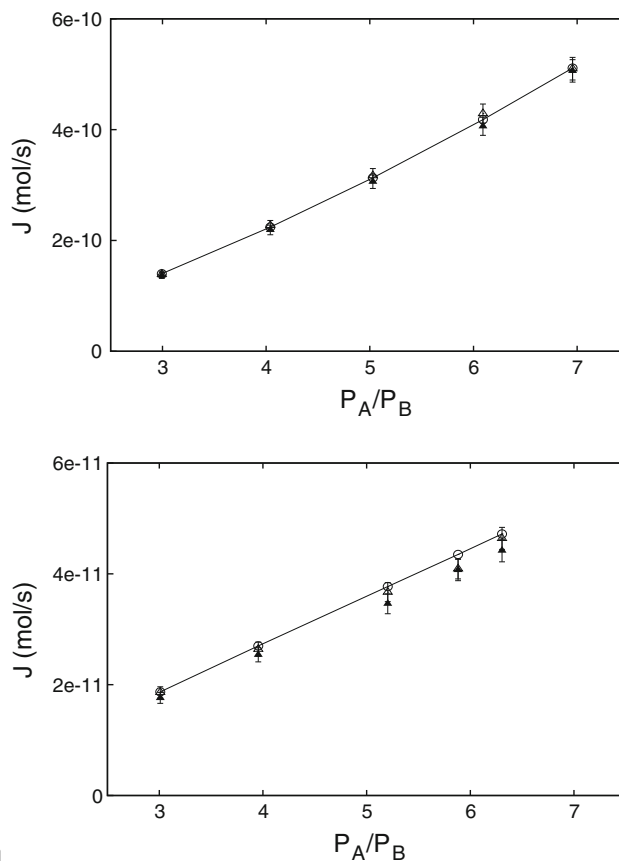


Fig. 3 Computational and experimental total molar flow rates of He-Ar ($C_A = 0.9014$), with (i) $P_B \approx 15$ kPa (up) and (ii) $P_B \approx 2$ kPa (down). The symbols open circle, open triangle, and filled triangle represent $J, J_A^c,$ and $J_B^c,$ respectively. The solid line is plotted to guide the eyes for the computational results of J

570 results, while for $P_B \approx 2$ kPa, in some cases, they are
 571 within the experimental uncertainties and, in other cases,
 572 they are at the upper margin of the experimental dispersion
 573 bars. This behavior is attributed to the fact that both
 574 experimental uncertainties and kinetic modeling errors are
 575 increased as the gas rarefaction is increased. In particular,
 576 based on the above discussion, it is clear that the experi-
 577 mental uncertainties, mainly due to outgassing, are reduced
 578 in the case of higher downstream pressure $P_B \approx 15$ kPa.
 579 Also, in this case, since the gas is more dense, the flow lies
 580 in the slip or early transition region, and the McCormack
 581 model description provides a more accurate description of
 582 the transport coefficients and the flow field. In the case of
 583 lower downstream pressure $P_B \approx 2$ kPa, the gas is more
 584 dilute and the increased rarefaction may introduce some
 585 mismatch between the McCormack model and the true
 586 experimental results. However, the overall deviation
 587 between computational and experimental results is within
 588 the introduced modeling and measurement uncertainties
 589 and, therefore, it is considered as very good.

590 As mentioned before, the computational approach in
 591 addition to the molar flow rates yields the pressure and
 592 concentration distributions along the channel. Some typical
 593 results of the axial distributions $P(z'/L)/P_B$ and $C(z'/L)$ are
 594 shown in Figs. 4 and 5 for $P_B \approx 15$ kPa and $P_B \approx 2$ kPa,
 595 respectively. These data correspond to the case of
 596 $C_A = 0.5$ in Table 1, with each plot in the figures corre-
 597 sponding to a given pressure ratio. The inlet and outlet
 598 values are, for the pressure distribution $P(0) = P_A/P_B$ and
 599 $P(1) = 1$ and for the concentration distribution $C(0) =$
 600 $C(1) = 0.5$. The pressure distributions have a qualitative
 601 behavior, which is similar to the one observed in pressure-
 602 driven single gas flow configurations (Varoutis et al. 2009).
 603 They are linear in highly rarefied atmospheres, and then
 604 they are gradually converted to nonlinear as the atmosphere
 605 becomes less rarefied. Next, turning to the concentration
 606 distributions, it is clearly seen that they are non-uniform
 607 along the channel. Both in Figs. 4 and 5, starting from the
 608 inlet point, the concentration decreases, taking its mini-
 609 mum value of $C \approx 0.45$ somewhere at the second half of

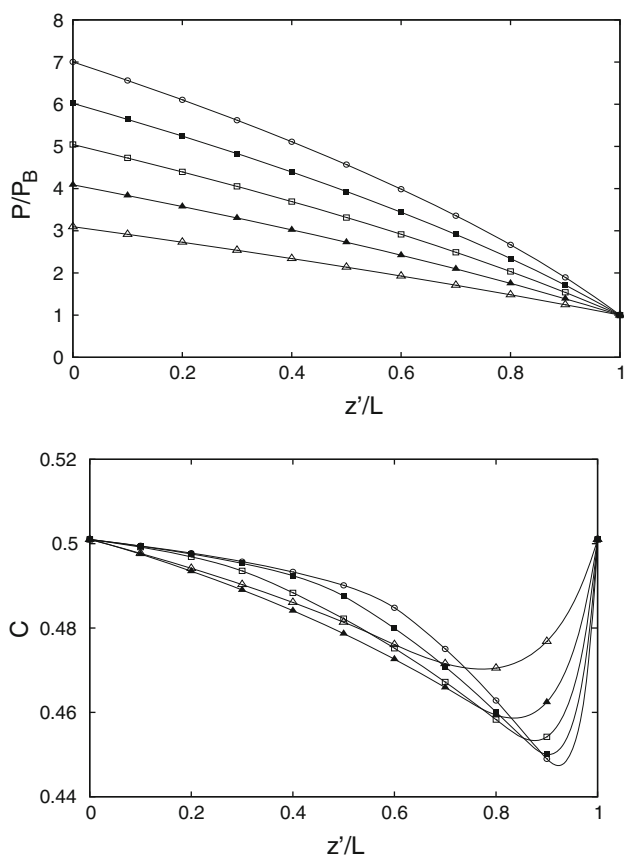


Fig. 4 Distributions of normalized pressure (*up*) and concentration (*down*) for He–Ar ($C_A = 0.5010$) along the channel, with $P_B \approx 2$ kPa. The symbols *open triangle*, *filled triangle*, *open square*, *filled square*, and *open circle* correspond to results for $P_A/P_B = [3.01, 4.09, 5.04, 6.02, \text{ and } 7.00]$, respectively

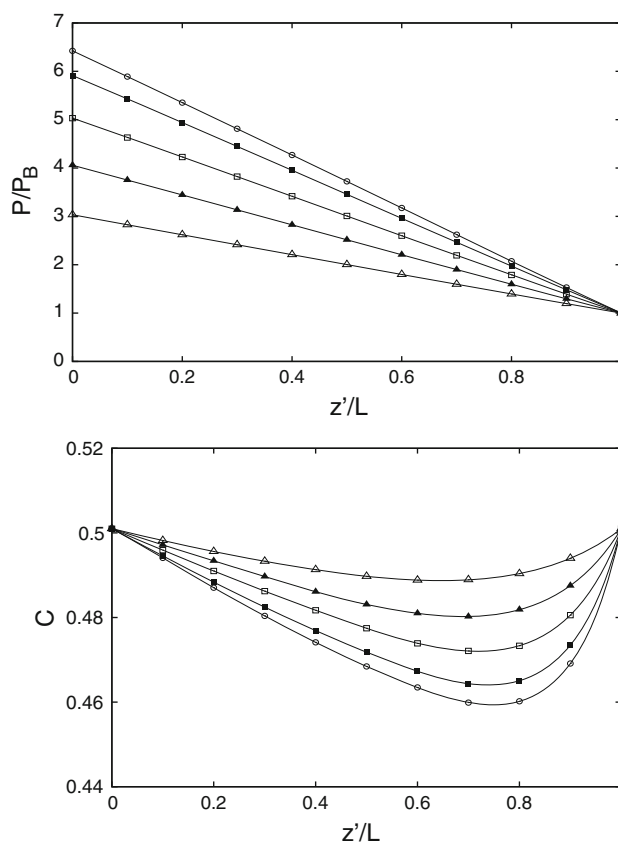


Fig. 5 Distributions of normalized pressure (*up*) and concentration (*down*) for He–Ar ($C_A = 0.5010$) along the channel, with $P_B \approx 15$ kPa. The symbols *open triangle*, *filled triangle*, *open square*, *filled square*, and *open circle* correspond to results for $P_A/P_B = [3.03, 4.06, 5.03, 5.91, \text{ and } 6.42]$, respectively

the channel, and then it increases and reaches the outlet 610
 value. The point in the channel where the minimum value 611
 occurs is different for each pressure ratio and downstream 612
 pressure. Also, the qualitative behavior between the con- 613
 centration distributions for $P_B \approx 15$ kPa and $P_B \approx 2$ kPa 614
 is different, with the latter ones having a more smooth 615
 variation along the channel. The deviation of the concentra- 616
 tion from the uniform distribution is larger for the case 617
 $P_B \approx 2$ kPa. In this situation, the gas is more dilute and 618
 the diffusion effects are more important resulting into the 619
 increased separation of the gaseous components. 620

6 Concluding remarks 621

The pressure-driven binary gas flow through a rectangular 622
 microchannel has been investigated both computationally 623
 and experimentally. The computational approach is based 624
 on the numerical solution of the McCormack kinetic model 625
 and the experimental approach on the Constant Volume 626
 method. Based on the computed and measured total molar 627

628 flow rates, a systematic and detailed comparison has been
629 performed finding very good agreement in a wide range of
630 the Knudsen numbers inside the transition regime. This
631 outcome clearly demonstrates that the McCormack model
632 and the associated numeric scheme can be successfully
633 implemented to simulate pressure-driven microflows of
634 gaseous mixtures, providing accurate results with modest
635 computational effort. This remark is important taking into
636 account the feasibility of the theoretical–computational
637 scheme to easily provide solutions to other micro-flow
638 configurations and even more its potential to investigate
639 complex non-equilibrium phenomena such as diffusion
640 effects.

641 **Acknowledgment** The research leading to these results has
642 received funding from the European Community's Seventh Frame-
643 work Programme (FP7/2007–2013) under grant agreement no 215504.

644 References

- 645 Aoki K (2001) Dynamics of rarefied gas flows: asymptotic and
646 numerical analyses of the Boltzmann equation. In: 39th AIAA
647 aerospace science meeting and exhibit, Reno, 2001-0874
648 Bird GA (1994) Molecular gas dynamics and the direct simulation of
649 gas flows. Oxford University Press, Oxford
650 Breyiannis G, Varoutis S, Valougeorgis D (2008) Rarefied gas flow in
651 concentric annular tube: estimation of the Poiseuille number and
652 the exact hydraulic diameter. *Eur J Mech B Fluids* 27:609–622
653 Cercignani C (1988) The Boltzmann equation and its application.
654 Springer-Verlag, New York
655 Colin S (2005) Rarefaction and compressibility effects on steady and
656 transient gas flows in microchannels. *Microfluid Nanofluidics*
657 1:268–279
658 Colin S, Lalonde P, Caen R (2004) Validation of a second-order slip
659 flow model in rectangular microchannels. *Heat Transf Eng*
660 25:23–30
661 De Groot SR, Mazur P (1984) Non-equilibrium thermodynamics.
662 Dover, New York
663 Ewart T, Perrier P, Graur I, Méolans JG (2006) Mass flow rate
664 measurements in gas micro flow. *Exp Fluids* 41:487–498
665 Ewart T, Perrier P, Graur IA, Méolans JG (2007) Mass flow rate
666 measurements in a microchannel, from hydrodynamic to near
667 free molecular regimes. *J Fluid Mech* 584:337–356
668 Ferziger JH, Kaper HG (1972) Mathematical theory of transport
669 processes in gases. North Holland, Amsterdam
670 Harley JC, Huang Y, Bau HH, Zemel JN (1995) Gas flow in micro-
671 channels. *J Fluid Mech* 284:257–274
672 Ho CM, Tai YC (1998) Micro-electro-mechanical-systems (MEMS)
673 and fluid flows. *Annu Rev Fluid Mech* 30:579–612
674 Ivchenko IN, Loyalka SK, Tompson RV (1997) Slip coefficients for
675 binary gas mixture. *J Vac Sci Technol A* 15:2375–2381
676 Kandlikar SG, Garimella S, Li D, Colin S, King MR (2006) Heat
677 transfer and fluid flow in minichannels and microchannels.
678 Elsevier, Oxford
679 Kestin J, Knierim K, Mason EA, Naja B, Ro ST, Waldman M
680 (1984) Equilibrium and transport properties of the noble gases
681 and their mixture at low densities. *J Phys Chem Ref Data*
682 13:229–303
683 Kosuge S, Takata S (2008) Database for flows of binary mixtures
684 through a plane microchannel. *Eur J Mech B Fluids* 27:444–465

- Lockerby DA, Reese JM (2008) On the modelling of isothermal gas
685 flows at the microscale. *J Fluid Mech* 604:235–261
686
687 Marino L (2009) Experiments on rarefied gas flows through tubes.
688 *Microfluid Nanofluidics* 6:109–119
689 Maurer J, Tabeling P, Joseph P, Willaime H (2003) Second-order slip
690 laws in microchannels for helium and nitrogen. *Phys Fluids*
691 15:2613–2621
692 McCormack FJ (1973) Construction of linearized kinetic models for
693 gaseous mixtures and molecular gases. *Phys Fluids* 16:2095–
694 2105
695 Morini GL, Lorenzini M, Spiga M (2005) A criterion for experimen-
696 tal validation of slip-flow models for incompressible rarefied
697 gases through microchannels. *Microfluid Nanofluidics* 1:190–
698 196
699 Naris S, Valougeorgis D, Kalempa D, Sharipov F (2004a) Discrete
700 velocity modelling of gaseous mixture flows in MEMS. *Super-
701 lattices Microstruct* 35:629–643
702 Naris S, Valougeorgis D, Kalempa D, Sharipov F (2004b) Gaseous
703 mixture flow between two parallel plates in the whole range of
704 the gas rarefaction. *Physica A* 336:294–318
705 Naris S, Valougeorgis D, Kalempa D, Sharipov F (2005) Flow of
706 gaseous mixtures through rectangular microchannels driven by
707 pressure, temperature and concentration gradients. *Phys Fluids*
708 17:100607.1–100607.12
709 Pitakarnnop J (2009) Analyse expérimentale et simulation numérique
710 d'écoulements raréfiés de gaz simples et de mélanges gazeux
711 dans les microcanaux. Ph.D. thesis, University of Toulouse
712 Pitakarnnop J, Geoffroy S, Colin S, Baldas L (2008) Slip flow in
713 triangular and trapezoidal microchannels. *Int J Heat Technol*
714 26:167–174
715 Pitakarnnop J, Varoutis S, Valougeorgis D, Geoffroy S, Baldas L,
716 Colin S (2010) A novel experimental setup for gas microflows.
717 *Microfluid Nanofluidics* 8:57–72
718 Sharipov F (1994) Onsager-Casimir reciprocity relations for open
719 gaseous systems at arbitrary rarefaction III. Theory and its
720 application for gaseous mixtures. *Physica A* 209:457–476
721 Sharipov F (1999) Rarefied gas flow through a long rectangular
722 channel. *J Vac Sci Technol A* 17:3062–3066
723 Sharipov F, Seleznev V (1998) Data on internal rarefied gas flows. *J
724 Phys Chem Ref Data* 27:657–706
725 Sharipov F, Kalempa D (2002) Gaseous mixture flow through a long tube
726 at arbitrary Knudsen number. *J Vac Sci Technol A* 20:814–822
727 Sharipov F, Kalempa D (2003) Velocity slip and temperature jump
728 coefficients for gaseous mixtures. I. Viscous slip problem. *Phys
729 Fluids* 15:1800–1806
730 Sharipov F, Kalempa D (2005) Separation phenomena for gaseous
731 mixture flowing through a long tube into vacuum. *Phys Fluids*
732 17:127102.1–127102.8
733 Siewert CE, Valougeorgis D (2004) The McCormack model: channel
734 flow of a binary gas mixture driven by temperature, pressure and
735 density gradients. *Eur J Mech B Fluids* 23:645–664
736 Szalmas L (2007) Multiple-relaxation time lattice Boltzmann method
737 for the finite Knudsen number region. *Physica A* 379:401–408
738 Szalmas L, Valougeorgis D (2010) Rarefied gas flow of binary
739 mixtures through long channels with triangular and trapezoidal
740 cross sections. *Microfluid Nanofluidics*. doi:10.1007/s10404-
741 010-0564-9
742 Takata S, Yasuda S, Kosuge S, Aoki K (2003) Numerical analysis of
743 thermal-slip and diffusion-slip flows of a binary mixture of hard-
744 sphere molecular gases. *Phys Fluids* 15:3745–3766
745 Takata S, Sugimoto H, Kosuge S (2007) Gas separation by means of
746 the Knudsen compressor. *Eur J Mech B Fluids* 26:155–181
747 Valougeorgis D, Naris S (2003) Acceleration schemes of the discrete
748 velocity method: gaseous flows in rectangular microchannels.
749 *SIAM J Sci Comput* 25:534–552

- 750 Varoutis S, Naris S, Hauer V, Day C, Valougeorgis D (2009) 757
751 Computational and experimental study of gas flows through long 758
752 channels of various cross sections in the whole range of the 759
753 Knudsen number. J Vac Sci Technol A 27:89–100 760
754 Wagner W (1992) A convergence proof for Bird direct simulation
755 Monte Carlo method for the Boltzmann equation. J Stat Phys
756 66:1011–1044
- Zohar Y, Lee SYK, Lee WY, Jiang L, Tong P (2002) Subsonic gas
flow in a straight and uniform microchannel. J Fluid Mech
472:125–151

UNCORRECTED PROOF